IEEE Photonics Journal
An IEEE Photonics Society Publication

Open Access

Influence of Subwavelength Grating Asymmetry on Long-Wavelength Infrared Transmittance Filters

Volume 10, Number 6, December 2018

Michael Barrow
Marty Scherr
Jamie Phillips

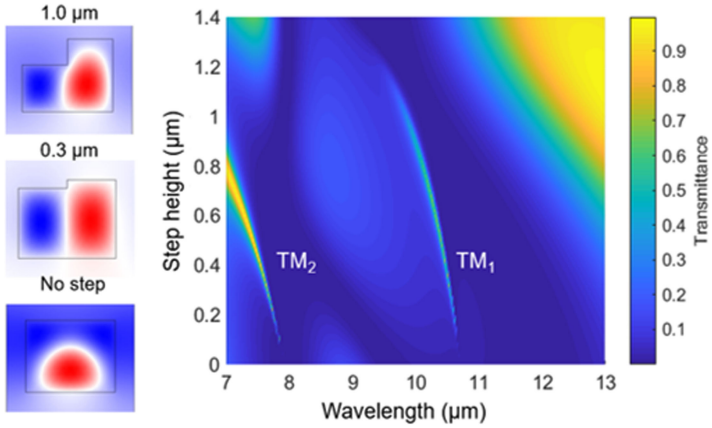

DOI: 10.1109/JPHOT.2018.2881478
1943-0655

Influence of Subwavelength Grating Asymmetry on Long-Wavelength Infrared Transmittance Filters

Michael Barrow, Marty Scherr, and Jamie Phillips

Department of Electrical Engineering and Computer Science, University of Michigan, Ann Arbor, MI 48109 USA

DOI:10.1109/JPHOT.2018.2881478

Manuscript received October 10, 2018; accepted November 12, 2018. Date of publication November 15, 2018; date of current version November 27, 2018. Corresponding author: Michael Barrow (e-mail: barrowm@umich.edu).

Abstract: Subwavelength dielectric gratings provide a means of narrowband spectral filtering by coupling to quasi-guided leaky modes, providing a high reflectivity background and narrowband transmittance via Fano resonance behavior. Geometrically asymmetric two-step gratings enable normal incidence filtering by accessing symmetry-protected leaky modes. The impact of asymmetry on leaky mode coupling and optical filter response are studied via simulation and described by the Fano resonance theory. The influence of asymmetry introduced by grating step height and angular cone of incidence are verified experimentally in silicon/air gratings in the long-wavelength infrared (8–14 μm).

Index Terms: Gratings, hyperspectral imaging, subwavelength structures.

1. Introduction

Spectral filters are indispensable optical components across many fields, including astronomy, climate science, surveillance, and thermal imaging. These applications frequently require operation within the long-wavelength infrared (LWIR, 8–14 μm) spectral region. Infrared systems in the LWIR are a necessity due to terrestrial black body emission and the high-transmittance window in the Earth's atmosphere in this wavelength band. For many applications, such as spectroscopy and hyperspectral-imaging, narrow spectral bands need to be resolved. Toward this end, subwavelength dielectric gratings (SWG) provide an effective method to filter optical spectra while being relatively simple to fabricate and operate. The relative simplicity of SWG geometry is particularly advantageous in the LWIR in comparison to the thickness requirements for filters based on Fabry-Pérot etalon or Bragg reflector structures. Using SWG structures, researchers have demonstrated focusing lenses [1], [2], broadband reflectors [3]–[5], notch filters [6], [7], color filters [8], narrowband transmission filters [9]–[13], amongst other devices.

Spectral filtering may be achieved in SWGs via coupling to guided mode resonances [14]. These resonances, associated with leaky modes, propagate within the gratings as Bloch waves while radiating into the continuum of radiative states. Interference between a grating mode and directly transmitted light yields an asymmetric Fano lineshape. The transmittance minimum of a strongly coupled leaky mode provides a broad, high-reflectivity background. By weakly coupling to another leaky mode, SWGs yield a narrow band-pass response. Proper geometric design positions the

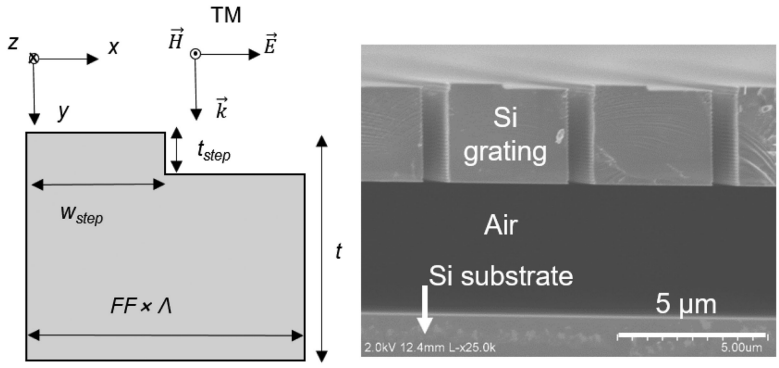

Fig. 1. Schematic drawing of asymmetric two-step dielectric gratings and cross-sectional scanning electron microscopy image of a fabricated structure in silicon.

narrow transmittance band within the high-reflectivity background, providing a desirable spectral response for a filter. Foteinopoulou *et al.* demonstrated strong leaky mode coupling between incident light and photonic crystal surface modes when the modal profile is antisymmetric upon reflection in the yz-plane (as defined in Fig. 1) [15]. However, a normally incident plane wave possesses even-symmetry, prohibiting coupling to modes with odd modal symmetry. Despite their nonzero state density, photonic lattices exhibit bands of near-total reflection when the symmetries of the leaky mode and incident plane wave are accordingly mismatched [16]. For coupling to occur, the field overlap integral between the incident light and leaky mode must be non-zero. An asymmetric "two-step" grating geometry may be used to relax the symmetry condition to enable coupling at normal incidence [17]. Introduction of the step breaks the x-symmetry of the leaky mode, ensuring a non-zero field overlap with the incident light. Cui *et al.* [18] numerically evaluated asymmetric zero contrast grating filters [19], establishing an inverse relationship between geometric asymmetry and transmittance peak linewidth. However, while the use of asymmetry to enable normal incidence coupling has been demonstrated, an understanding of the relationships between asymmetry, coupling strength, and filter resonance characteristics are not well understood. Similar studies [18], [20] ignore resonant peak transmittance, an integral parameter in transmission filter design. This work explores details of leaky mode coupling in asymmetric two-step SWGs via simulated and experimental data. Further, we present a means to optimize asymmetry in normal-incidence grating filter design.

2. Numerical and Experimental Methods

The two-step SWGs are based on the high contrast grating (HCG) scheme [21], utilizing a high refractive index contrast between the silicon dielectric grating and air, the surrounding medium. A schematic diagram and cross-sectional scanning electron microscope of the gratings are shown in Fig. 1, consisting of silicon grating bars surrounded by air, and suspended 4 μm above a silicon substrate. The relevant geometric parameters are the period Λ, the fill factor *FF*, the grating thickness *t*, the step height t_{step}, and the step width w_{step}. Transverse magnetic (TM) polarization is defined with the magnetic field along the grating.

Optical response of the gratings was simulated using finite element methods implemented in COMSOL Multiphysics. The SWGs were modeled using a two-dimensional grating cross section, with x-direction periodicity enforced via Floquet boundary conditions and port defined several microns above the gratings with an incident TM-polarized plane wave. Spectral transmittance simulations were used to optimize the gratings by parametrically sweeping the grating period, fill factor, and thickness. To reduce the design space, the step width was fixed at $(\Lambda)(FF)/2$. A well-optimized geometry produces a broad ($\Delta\lambda/\lambda \approx 0.25$) high reflectivity ($R > 95\%$) band with a transmittance peak near the center of the band. As demonstrated previously [17], the period and fill factor may

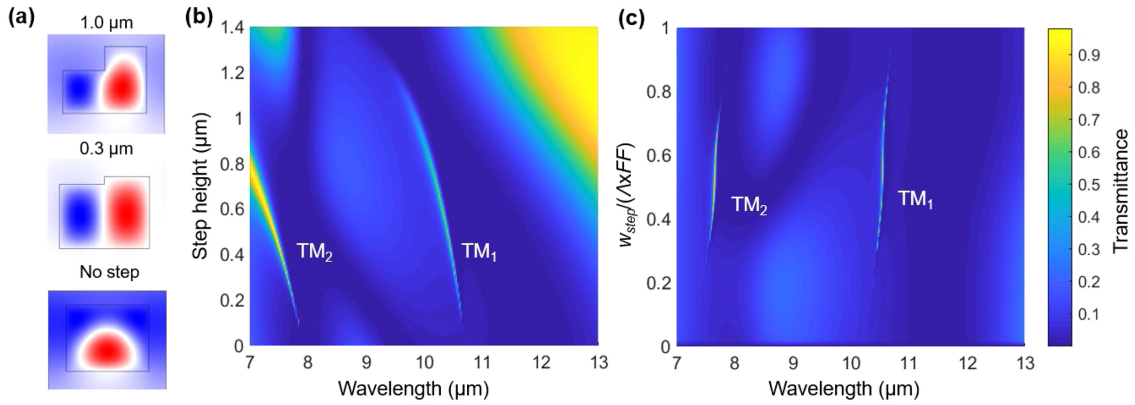

Fig. 2. (a) H_z-field intensity of leaky mode TM_1 for three example step heights at normal incidence. (b) Simulated normal incidence transmittance spectra of an asymmetric two-step HCG as a function of step height. The geometric parameters are $\Lambda = 4.2\ \mu$m, $FF = 0.79$, $t = 2.8\ \mu$m, and $w_{step} = 1.66\ \mu$m. (c) Simulated transmittance spectra as a function of w_{step} normalized to the grating width. The geometric parameters are the same as in Fig. 2(b) with $t_{step} = 0.3\ \mu$m.

be judiciously chosen to tune the location of the transmittance peak, allowing specific wavelengths to be filtered. The numerical studies in this report use optical constants obtained from [22].

Gratings were realized experimentally using commercial silicon on insulator (SOI) wafers. To achieve the desired grating thickness, a blanket etch was used to thin the top silicon layer. Next, a Bosch dry etch process was used to anisotropically define trenches between the grating bars. This same process is repeated to etch the lower step of the grating. Although the Bosch process produces visible sidewall scalloping, this feature has not been found to be detrimental to the optical response. Lastly, a hydrofluoric acid wet etch is used to remove the buried oxide layer to release the suspended gratings. The transmittance spectra of the fabricated gratings were measured using Fourier transform infrared spectroscopy (FTIR) and a gold wiregrid polarizer to define polarization of incident light. A microscope accessory interfaced with the FTIR was used to focus to a spot size of approximately 100 μm using Cassegrain optics with obliquely incident light over a range of 20–38°. To obtain conditions approximating normal incidence, the gratings are placed on a 20° inclined sample holder, including an additional iris diaphragm placed in the incident optical path to limit the cone of incident angles.

3. Filter *Q*-Factor Dependence on Asymmetry

The transmittance spectra of the asymmetric two-step gratings at normal incidence are fundamentally similar to those of symmetric rectangular gratings under oblique incidence. As shown in the simulated transmittance spectra of Fig. 2(b), the gratings produce a broad reflectance background for all step heights. As the step is introduced, the symmetry condition is relaxed, and narrow transmittance peaks appear. For large step heights the peak transmittance approaches unity (>95%). Fig. 2(a) shows the H_z-field intensity for several representative step heights at normal incidence. As predicted by symmetry arguments, the symmetric grating does not enable normal incidence filtering, nor does it exhibit the antisymmetric TM_1 modal profile. When the step height approaches approximately half the grating thickness, the two-step grating is no longer a small perturbation of the rectangular grating geometry. Consequently, the narrowband TM mode associated with the rectangular grating ceases to exist for very deep step heights. Fig. 2(c) shows the simulated transmittance spectra as a function of the grating step width. The peak intensity is greatest when the step width is half the grating width, at which point coupling is strongest. As w_{step} moves away from ΛxFF/2, the coupling strength decreases until the grating is fully symmetric and coupling is prohibited. Accordingly, it is possible to tune the leaky mode coupling strength via w_{step}. The maximum strength is thus governed by t_{step}.

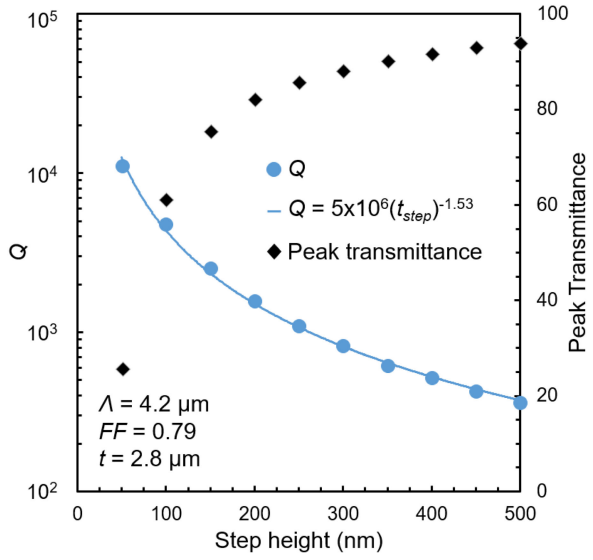

Fig. 3. Dependence of *Q*-factor on grating step height for simulated transmittance spectra and *Q*-factor defined by peak linewidth ($\Delta\omega$ via FWHM, blue circles). The relationship between step height and peak transmittance is also shown (black diamonds).

At normal incidence, the asymmetry is solely determined by the grating step height. A larger degree of asymmetry increases the field overlap between the leaky mode and an incident plane wave, enabling stronger coupling to the radiative modes and subsequent faster energy decay of the coupled mode to the continuum. Analogous to lifetime broadening, higher energy decay rates result in spectral broadening where the transmittance peak linewidth has a strong dependence on grating step height. The underlying physical mechanism of the observed narrowband response may be described by a Fano resonance, consisting of discrete weakly coupled leaky modes interacting with the continuum of radiative modes associated with the broad high-reflectivity background. This is further evidenced by the characteristic asymmetric lineshape of the simulated transmittance peaks. The Fano transmittance (T_{Fano}), which resembles the general expression of the Fano lineshape, is given by

$$T_{Fano} = |t_D|^2 \frac{(q+\delta)^2}{1+\delta^2} \tag{1}$$

where, t_D is the non-resonant transmission probability, q denotes the asymmetry factor due to interference between the discrete mode and the continuum, ω_0 is the resonance frequency, $\delta = (\omega - \omega_0)/\gamma$ is the reduced frequency, and γ is the total energy decay rate.

Narrowband filter performance is characterized by its quality factor (*Q*-factor, or *Q*). We compare two definitions of *Q*: 1) $Q = \omega_0/\Delta\omega$, where ω_0 is the resonance frequency, and $\Delta\omega$ is the full width at half maximum (FWHM) of the transmittance peak and 2) $Q = \omega_0/2\gamma$, where ω_0 is the resonance frequency and γ is the resonant energy decay rate obtained by Fano lineshape fitting. The *Q*-factor demonstrates a clear dependence on grating step height shown by the extracted values for *Q* (Fig. 3) from simulated transmittance spectra, for which data extraction shows close agreement for both definitions of *Q*. The observed reduction in *Q* with increasing step height supports the hypothesis of increased leaky mode coupling strength with the introduction of grating asymmetry, and corresponding broadening of the transmittance peak linewidth.

The transmittance spectrum and *Q*-factor of the two-step grating is strongly dependent on resonant loss due to material absorption and/or scattering. The Fano resonance description may be modified to account for these losses [24], given by

$$T(\delta) = \eta_{rad} T_{Fano}(\delta) - \beta \frac{\eta_{rad}\eta_{abs}}{1+\delta^2} + \eta_{abs}|t_D|^2 \tag{2}$$

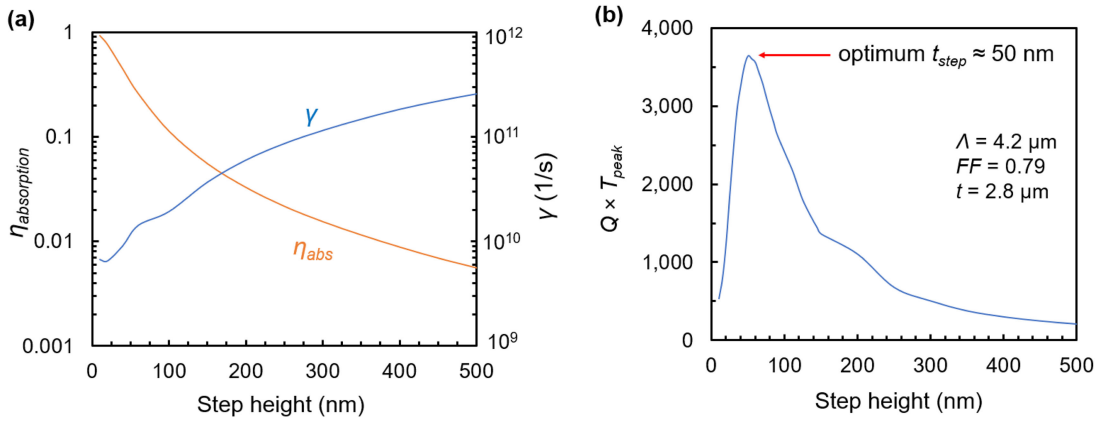

Fig. 4. (a) Tradeoff between leaky mode decay rate and absorption probability (b) Simulated Figure of merit ($Q \times$ peak transmittance) used to determine optimum step height.

where η_{rad} is the resonant radiation probability η_{abs} is the material absorption probability ($\eta_{abs} = 1 - \eta_{rad}$), $\beta = 4\eta_1\eta_2/(\eta_1 + \eta_2)^2$ is the coupling symmetry factor, and η_1 and η_2 are the resonant transmittance and reflection probabilities.

In practice, the utility of the spectral filter depends on both the Q-factor and the contrast of peak transmittance relative to the background. Q defines the spectral resolution of the filter, while the peak contrast determines the signal to noise ratio. For very small step heights, a lossless filter may theoretically exhibit arbitrarily high Q, for an ideal dielectric, with actual Q determined by material loss (i.e., $1/Q_{tot} = 1/Q_{loss} + 1/Q_{rad}$). Although silicon is mostly transparent at LWIR wavelengths, energy is lost to multiphonon absorption [23]. The published LWIR extinction coefficient for silicon is on the order of 1×10^{-4} in the LWIR [22], [23], suggesting that material absorption may have a minimal effect. However, significant losses may result for even small values of material absorption or scattering due to resonance enhancement [24]. A further intuitive description is optical confinement in the leaky mode, where reduced decay rate will lead to higher absorption probability. Utilizing the model in Eq. 2 to fit simulated transmittance spectra (including silicon extinction coefficients interpolated from Reference 22) extracted parameters for absorption probability and leaky mode decay rate as function of step height are shown in Fig. 4(a), illustrating the relationship between decay rate and absorption probability. For cases of sufficient coupling strength, occurring at small step height, there is a tradeoff in achieving optimal filter behavior. While smaller step height results in high Q, this must be balanced with the increased absorption probability that degrades peak transmittance. An approximate figure of merit may be defined by the product of peak transmittance and Q, with resulting dependence on SWG step height shown in Fig. 4(b). An optimum step height for a given geometry occurs at approximately 2% of the grating thickness. Increased absorption losses would shift the optimum step height to larger values.

4. Experimental Results and Analysis of Non-Idealities

Experimental transmittance spectra for asymmetric two-step gratings with variable step height are shown in Fig. 5, with nominal grating parameters of $\Lambda = [4.0, 4.2, 4.4, 4.6, 4.8, 5.0]$ μm, $FF = [0.70, 0.74, 0.78, 0.82, 0.86]$, $t = 2.95$ μm, and $w_{step} = 0.5(\Lambda)(FF)$. Broader transmittance peaks are observed with increased step height, as predicted by simulation, and agreeing with the hypothesis that coupling strength increases with step height. The experimental values for Q and peak transmittance of the fabricated gratings are substantially lower than predicted from simulation. This discrepancy may be attributed to several factors including the non-ideal range of incident angles associated with the FTIR instrumentation, geometric parameter variations, sidewall scalloping, material defects produced by the fabrication process (e.g., surface states), and grating size. For gratings suspended 4 μm above a silicon substrate, approximately 30% of the peak transmittance

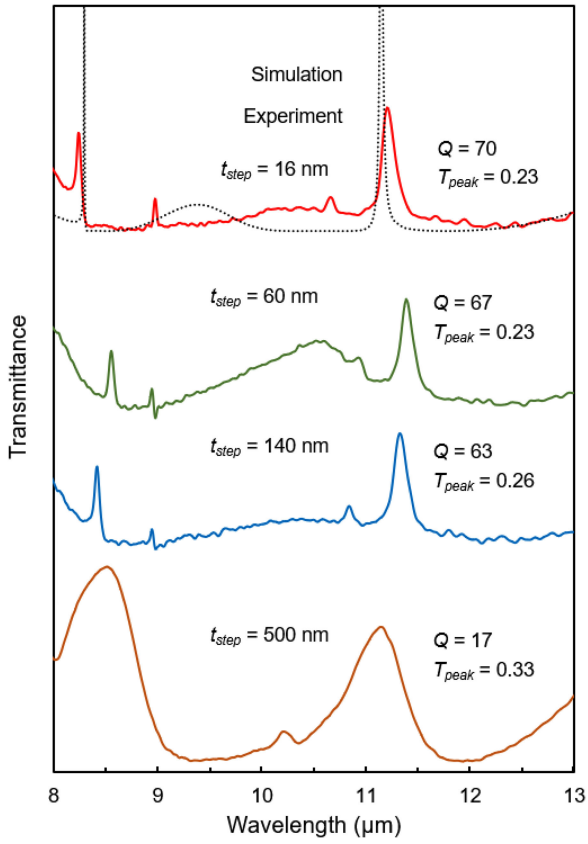

Fig. 5. Experimentally obtained transmission spectra for asymmetric subwavelength gratings of varying step heights. The geometric parameters are $\Lambda = 5.0\ \mu$m, $FF = 0.70$, $t = 2.95\ \mu$m, and $w_{step} = 1.75\ \mu$m.

will be lost due to reflection at the air/substrate interface. Transmittance measurements on the 500 μm silicon handle layer alone suggest that handle layer absorption is not the primary cause of the low measured transmittance peak. The deleterious effect of finite grating size on peak transmittance and Q is well established [25], [26]. Since the measured gratings only contain 35 periods, this is likely a significant source of loss. Therefore, we attribute the remaining loss to the non-idealities listed above. For gratings with the same parameters as in Fig. 5, with $t_{step} = 60$ nm, and a 0–5° cone of incident light, numerical calculations predict a Q of approximately 500. This calculated value mostly corresponds to radiative loss, given the strong leaky mode coupling. Therefore, since the measured value of Q was 67, experimental non-idealities drastically limited Q_{loss} to approximately 75. The broadened peak for a step height of 500 nm is consistent with reduction in Q due to grating asymmetry. The Q for smaller step heights measured for the 16–140 nm range are all very similar. This lack of dependence of Q on step height may be interpreted as a region where measured transmittance is dominated by the range of angular incidence of the FTIR instrumentation, rather than by the inherent limitation of the filter Q for pure normal incidence conditions. Although experimental limitations prevent a true demonstration of leaky mode coupling at normal incidence, Fig. 5 reveals the expected relationship between step height, Q, and peak transmittance (i.e., the coupling strength increases with step height).

To determine the influence of the angular range of the incident light, transmittance spectra for the grating with $t_{step} = 16$ nm in Fig. 5 was studied under varying cone of incident angles. The angular range was defined by adjusting the iris aperture in the optical path just prior to incidence on the gratings. The measured transmittance spectra demonstrate peak broadening for several ranges of incident angles (Fig. 6). The decrease in Q with larger angular range may be attributed to

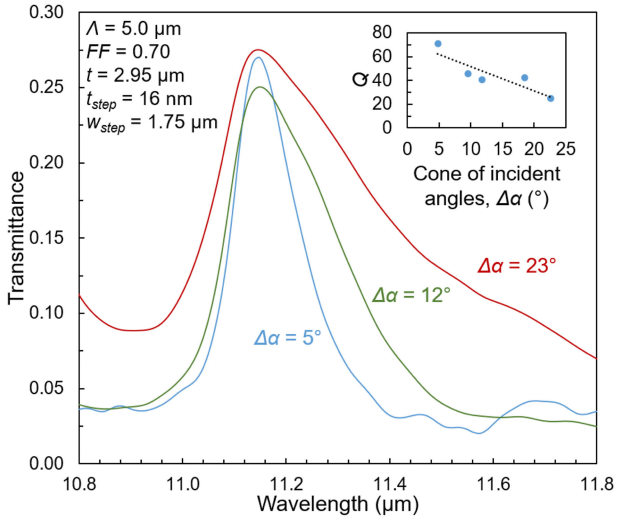

Fig. 6. Transmittance peak broadening due to range of incident angles in experimental characterization setup. (inset) Extracted Q for varying cones of incident angles.

a combination of two factors: 1) increased asymmetry leading to spectral broadening (analogous to increased step height), and 2) shift in spectral position of resonance for differing angles of incidence due to dispersion relations of the leaky modes, where the experimentally observed peak is a combination of a range of filter responses with varying resonant wavelengths.

5. Conclusions

In summary, introducing an asymmetric two-step grating geometry breaks the symmetry condition, enabling leaky mode coupling at normal incidence. The Q-factor of this peak is dependent on the step height of the two-step gratings, where larger step heights result in greater asymmetry and therefore stronger coupling. Accordingly, Q is reduced for greater step heights, presenting tradeoffs associated with peak transmittance, Q, and access to normal incidence response. The significant effect of resonance enhanced absorption is established for asymmetric SWGs based on Fano resonance behavior, highlighting the role of material absorption and scattering in determining filter performance. This work provides a physical description for narrowband filtering in SWGs, where filters may be optimized with appropriate inputs for material loss and incident cone of angles.

References

[1] D. Fattal, J. Li, Z. Peng, M. Fiorentino, and R. Beausoleil, "Flat dielectric grating reflectors with focusing abilities," *Nature Photon.*, vol. 4, pp. 466–470, 2010.
[2] C. Ma, Y. Huang, X. Duan, G. Dou, M. Mao, and X. Ren, "Polarization-insensitive focusing lens using 2D blocky high-contrast gratings," *IEEE Photon. Technol. Lett.*, vol. 27, no. 7, pp. 697–700, Apr. 2015.
[3] C. Mateus, M. Huang, L. Chen, C. Chang-Hasnain, and Y. Suzuki, "Broad-band mirror (1.12–1.62 μm) using a subwavelength grating," *IEEE Photon. Technol. Lett.*, vol. 16, no. 7, pp. 1676–1678, Jul. 2004.
[4] C. Chang-Hasnain and W. Yang, "High-contrast gratings for integrated optoelectronics," *Opt. Photon.*, vol. 4, pp. 379–440, 2012.
[5] L. Huang, D. Liang, J. Zeng, Y. Xiao, and H. Wu, "A broadband multilayered nonpolarization resonant reflector," *IEEE Photon.*, vol. 7, no. 4, Aug. 2015, Art. no. 6500306.
[6] D. Wang, Q. Wang, and D. Liu, "Polarization-insensitive filter for incidence between classic and full conical mountings," *IEEE Photon. Technol. Lett.*, vol. 30, no. 5, pp. 495–498, Mar. 2018.
[7] Y. Zhong *et al.*, "Mid-wave infrared narrow bandwidth guided mode resonance notch filter," *Opt. Lett.*, vol. 42, pp. 223–226, 2017.
[8] Y. Horie *et al.*, "Visible wavelength color filters using dielectric subwavelength gratings for backside-illuminated CMOS image sensor technologies," *Nano Lett.*, vol. 17, pp. 3159–3164, 2017.

[9] M. Niraula, J. Yoon, and R. Magnusson, "Single-layer optical bandpass filter technology," *Opt. Lett.*, vol. 40, pp. 5062–5065, 2015.
[10] A.-L. Fehrembach *et al.*, "2 $\times$ 1D crossed strongly modulated gratings for polarization independent tunable narrowband transmission filters," *J. Opt. Soc. Amer. A*, vol. 34, pp. 234–240, 2017.
[11] L. Mace, O. Gauthier-Lafaye, A. Monmayrant, and H. Camon, "Design of angularly tolerant zero-contrast grating filters for pixelated filtering in the mid-IR range," *J. Opt. Soc. Amer. A*, vol. 34, pp. 657–665, 2017.
[12] Y. Ko and R. Magnusson, "Flat-top bandpass filters enabled by cascaded resonant gratings," *Opt. Lett.*, vol. 41, pp. 4704–4707, 2016.
[13] Y. Ko, M. Niraula, and R. Magnusson, "Divergence-tolerant resonant bandpass filters," *Opt. Lett.*, vol. 41, pp. 3305–3308, 2016.
[14] S. Wang and R. Magnusson, "Theory and applications of guided-mode resonance filters," *Appl. Opt.*, vol. 32, pp. 2606–2613, 1993.
[15] S. Foteinopoulou *et al.*, "Experimental verification of backward wave propagation at photonic crystal surfaces," *Appl. Phys. Lett.*, vol. 91, 2007, Art. no. 214102.
[16] K. Sakoda, "Symmetry, degeneracy, and uncoupled modes in two-dimensional photonic lattices," *Phys. Rev. B*, vol. 52, pp. 7982–7986, 1995.
[17] M. Scherr, M. Barrow, and J. Phillips, "Long-wavelength infrared transmission filters via two-step subwavelength dielectric gratings," *Opt. Lett.*, vol. 42, pp. 518–521, 2017.
[18] X. Cui, H. Tian, G. Shi, and Z. Zhou, "Normal incidence filters using symmetry-protected modes in dielectric subwavelength gratings," *Sci. Rep.*, vol. 6, 2016, Art. no. 36066.
[19] R. Magnusson, "Wideband reflectors with zero-contrast gratings," *Opt. Lett.*, vol. 39, pp. 4337–4340, 2014.
[20] J. Foley and J. Phillips, "Normal incidence narrowband transmission filtering capabilities using symmetry-protected modes of a subwavelength, dielectric grating," *Opt. Lett.*, vol. 40, pp. 2637–2641, 2015.
[21] C. Mateus, M. Huang, Y. Deng, A. Neureuther, and C. Chang-Hasnain, "Ultrabroadband mirror using low-index cladded subwavelength grating," *IEEE Photon. Technol. Lett.*, vol. 16, no. 2, pp. 518–520, Feb. 2004.
[22] E. Palik, *Handbook of Optical Constants of Solids*. Amsterdam, The Netherlands: Elsevier, 1998.
[23] D. Chandler-Horowitz and P. Amirtharaj, "High-accuracy, midinfrared (450 cm-1 $<\omega<$ 4000 cm-1) refractive index values of silicon," *J. Appl. Phys.*, vol. 97, 2005, Art. no. 123526.
[24] J. Yoon and R. Magnusson, "Fano resonance formula for lossy two-port systems," *Opt. Exp.*, vol. 21, pp. 17751–17759, 2013.
[25] R. Boye and R. Kostuk, "Investigation of the effect of finite grating size on the performance of guided-mode resonance filters," *Appl. Opt.*, vol. 39, pp. 3649–3653, 2000.
[26] D. Peters, S. Kemme, and G. Hadley, "Effect of finite grating, waveguide width, and end-facet geometry on resonant subwavelength grating reflectivity," *Opt. Soc. Amer. A*, vol. 21, pp. 981–987, 2004.